Proxies for atmospheric circulation over the Amazon basin from the aerosol composition in a Nevado Illimani firn core, Bolivia

Filipe G. L. Lindau[1], Jefferson C. Simões[1,2], Michael Handley[2], Elena Korotkikh [2], Patrick Ginot [3], Rafael R. Ribeiro [1]

[1]Centro Polar e Climático, Universidade Federal do Rio Grande do Sul, Porto Alegre, 91501-970, Brazil
[2]Climate Change Institute, University of Maine, Orono, ME 04469, USA
[3]Univ. Grenoble Alpes, CNRS, IRD, Grenoble INP, IGE, 38000 Grenoble, France

Key Points:

- Enhanced low level jets over the Amazon basin in 2015 increased S and Mn EFs in Illimani
- The Mn EF record can be used as a new proxy for atmospheric circulation over the Amazon basin
- 21^{st} century Cr pollution over the Altiplano is lower than during the late 20^{th} century

Corresponding author: F. G. L. Lindau, filipe.lindau@outlook.com

Abstract

Current changes in tropical South America due to atmospheric warming, deforestation, and glacier retreat impact moisture and water exchange between the Amazon basin and the Andes. Thus, a deeper understanding of past atmospheric variability is crucial for developing strategies for climate and environmental change scenarios in this region. Within this context, we investigated an 18-year firn core drilled at the Illimani to interpret its aerosol composition (trace elements and major ions) in relation to seasonal processes, particularly atmospheric circulation over the Amazon basin. The resulting 21^{st}-century record showed reduced Cr contamination over the Altiplano in comparison to the late 20^{th} century, which was probably related to reduced emissions from mining activities. Sulfur records suggest the influence of volcanic eruptions in 2006 (Rabaul) and 2014 (Nyamuragira-Nyiragongo). Overall, the aerosol composition was mainly modulated by precipitation variability over the Altiplano at both annual and seasonal timescales. However, Mn was enriched due to strengthened low-level jets in the Amazon basin during the dry season, especially in 2015. This was corroborated by the reanalysis data. Furthermore, Mn, Co, and Fe showed an unprecedented peak in the record during the wet season of 2014, which was consistent with the arrival of a dust plume from Africa over Amazonia. Therefore, the Mn enrichment record can be used as a new proxy for obtaining information about the South American Low-Level Jet, and, when considered together with more elements, might also indicate snow layers that were possibly loaded with aerosols from Africa.

1 Introduction

Atmospheric mechanisms involving Amazon-Andes connectivity in terms of evapotranspiration, moisture transport, and local convection are of particular importance to better understand hydrological disruption (related to deforestation, glacier retreat, and climate change) over that region (Espinoza et al., 2020). Beyond supplying water vapor, Amazonia exports biogenic aerosols and ashes to tropical Andes glaciers through dominant easterly trade winds. This might impact glacier mass balance by reducing the snow albedo (de Magalhães et al., 2019), but may also be recorded in their snow layers as a natural archive of the biogeochemical cycles regulating forest and climate feedbacks. Aerosols emitted from the Amazon basin have already been detected in firn and ice cores recovered at Nevado Illimani (hereafter Illimani, 16°37′S, 67°46′W, 6350 m a.s.l., Figure 1) and used as a paleothermometer of tropical South America (Kellerhals et al., 2010). In addition, higher temperatures over the Amazon basin are related to events of biomass-burning, which increases the concentration of refractive black carbon in Illimani (Osmont et al., 2019). However, aerosols deposited at Illimani mainly reflect conditions over its main source, which is the Altiplano (Figure 1), obfuscating the contribution of biogenic and/or biomass-burning material (Correia et al., 2003; Lindau et al., 2020).

Moreover, low-level northeasterly flow over the Amazon basin was found to be related to the increased deposition of Amazon-sourced aerosol (more concentrated in nitrate and ammonium) in Quelccaya (13°54′S, 70°48′W, 5670 m a.s.l., Figure 1) (Thompson et al., 2013). This circulation, the South American Low-Level Jet (SALLJ), is a common feature of the South American climate. The SALLJ delivers vast quantities of moisture originating in the Atlantic Ocean or in the Amazon basin over regions of Bolivia, Paraguay, and southern Brazil (Marengo, 2004). It is observed throughout the year and is a dominant feature of the South American Summer Monsoon (SAMS) (Vera et al., 2006). In addition, the Bolivian high, an upper tropospheric anticyclone located over Bolivia, is established during the mature phase of the SAMS, leading to upper tropospheric easterly winds that favor the transport of moist air from the Amazon lowlands toward the Altiplano (Lenters & Cook, 1997; Garreaud, 1999). However, since the onset of the 21^{st} century, interannual fluctuations of southern tropical Andes precipitation, which includes the Bolivian Altiplano, started to be more associated with strengthened low-level northerlies originating over the tropical North Atlantic, and less with upper-level easterly anomalies related to the Bolivian high (Segura et al., 2020). Moreover, the intensity and fre-

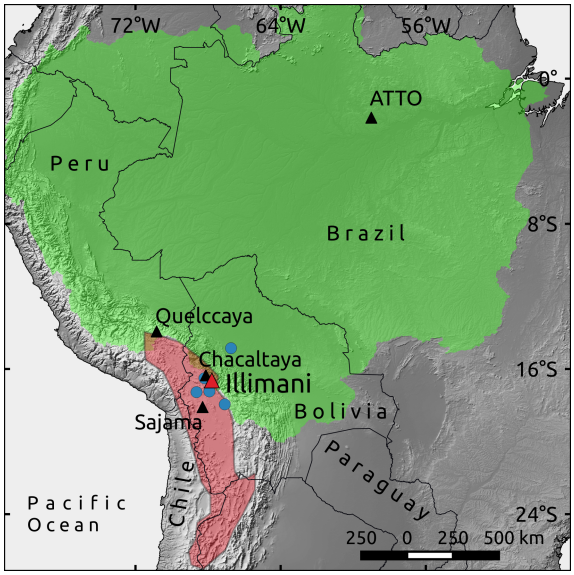

Figure 1. Location of Illimani (red triangle) whose records were compared to ice core (Quelccaya and Sajama) and atmospheric (Chacaltaya and ATTO) data (black triangles). Blue dots indicate the meteorological stations that provided precipitation data. Green and red areas delimit the Amazon basin and the Altiplano, respectively. The land basemap was obtained from Natural Earth (http://www.naturalearthdata.com).

quency of the SALLJ have shown an increase in the last decades in most seasons, increasing precipitation in the eastern Andes of Bolivia (Jones, 2019).

Considering that ice cores from the southern tropical Andes store high-resolution information over the last millennia (Vimeux et al., 2009), a high temporal resolution record of the aerosol composition during the current period of accentuated climate variability might be valuable for further analyzing these changes over a longer timeframe. Therefore, we will relate atmospheric observations over both the Altiplano and the Amazon basin, with the composition of the aerosol deposited at Illimani, by analyzing the elemental and ionic composition of a firn core spanning the 1999–2016 period.

2 Methods

2.1 Field Campaign and Firn Core Sampling

In June 2017, a 23.8 m firn core (IL2017) with a diameter of 10 cm was retrieved at an altitude of 6350 m a.s.l. on the saddle between the two Illimani summits, approximately where two deep ice cores were drilled in June 1999 (IL1999) (Knüsel et al., 2003). The expedition was coordinated by a French, Russian, Bolivian, and Brazilian team and integrated the Ice Memory project (Université Grenoble Alpes Foundation). After the drilling campaign, the container was shipped to the Institut des Géosciences de l'Environnement (IGE, Université Grenoble Alpes, France), where the core sections were weighed and cut longitudinally using a vertical band saw in a cold room (at -20°C). One quarter of the original core was used for dust analysis at EuroCold (University of Milano-Bicocca, Italy). Another quarter of the core was shipped in a frozen state to the Climate Change Institute (CCI, University of Maine, USA) for isotopic, ionic, and elemental analyses.

At the CCI, in a cold room set at -20°C, sections of the core were cut longitudinally with a vertical band saw to separate the inner and outer parts. The inner part (used for ionic and elemental analysis) was decontaminated by scraping with a clean ceramic

knife under a laminar flow HEPA bench inside the cold room. Then, the decontaminated inner part was sampled using a continuous melter system (Osterberg et al., 2006) in an ISO 6 Class clean room, yielding 767 samples (mean sample resolution of 3 cm). The samples for elemental analysis were collected into acid-cleaned (Optima HNO_3) low-density polyethylene (LDPE) vials and acidified with double-distilled HNO_3. This procedure was conducted using an ISO 5 laminar flow HEPA bench. Samples were stored for acidification at room temperature for approximately 1 month. The dilution rate reached using this acidification method may vary depending on the element. Using samples from Huascarán and Quelccaya (Figure 1), Uglietti et al. (2014) obtained a mean final recovery for Al on the order of 10% of its total concentration; conversely, Pb, As, and Mn showed final recoveries of approximately 80% (Uglietti et al., 2014).

2.2 Firn Core Analysis and Proxy Determination

The concentrations of the major ions (Na^+, K^+, Mg^{2+}, Ca^{2+}, Cl^-, and SO_4^{2-}) were measured by ion chromatography (IC). We used a Thermo Scientific^{TM}Dionex^{TM}Ion Chromatograph ICS-6000 analytical system at the CCI. The method detection limit (MDL, Table 1) was defined as three times the standard deviation of the blank samples (MilliQ®water, 10 blank samples). Blank concentrations were subtracted from each measurement.

Concentrations for 28 elements were measured using the CCI Thermo Scientific ELEMENT 2 inductively coupled plasma sector field mass spectrometer (ICP-SFMS) coupled to an ESI model SC-4 autosampler. The ICP-SFMS was calibrated daily with five standards, and as a reference, we used the SLRS-4 certified water (National Resource Council, Canada). Blanks were prepared with MilliQ®water, and the method blank was subtracted from each sample. The MDLs for the studied elements are listed in Table 1.

Because concentrations are partially modulated by snow accumulation at the drilling site, which can dilute the dominant dry deposition of the chemical species, we calculated the enrichment factors (EFs). They are independent of changes in accumulation, reflecting variations in emission sources and/or transport (Gabrielli et al., 2020). The EF normalization was calculated for the studied elements according to:

$$EF(x) = \frac{\frac{[X]_{sample}}{[CrustalElement]_{sample}}}{\frac{[X]_{UCC}}{[CrustalElement]_{UCC}}} \quad (1)$$

where X is the element of interest, and the mean composition of the upper continental crust was obtained from Wedepohl (1995). We used Sr as a proxy for rock and soil dust, as its biogeochemical cycle is almost unaffected by anthropogenic activities (Sen & Peucker-Ehrenbrink, 2012). In addition, Sr is highly correlated with other lithogenic elements, such as Ba ($R^2 = 0.93$) and Ce ($R^2 = 0.88$), both of which have already been used as a crustal reference in tropical Andean ice cores (Hong et al., 2004; Eichler et al., 2015). Finally, Sr was precisely determined by ICP-SFMS (Table 1).

Furthermore, we calculated the $SO_4^{2-}exc$, which is considered to be a good proxy for atmospheric H_2SO_4, originating exclusively from the oxidation of SO_2 in the atmosphere (Schwikowski et al., 1999; De Angelis et al., 2003). $SO_4^{2-}exc$ is the gypsum-like fraction of sulfate; thus, the calculation considers that Ca^{2+} is entirely deposited as $CaSO_4$. We estimated the Cl^- present as HCl by calculating the Cl^-exc, in accordance with De Angelis et al. (2003):

$$Cl^-exc = (Cl^-_{total} - Cl^-_{soil}) - 1.7 * (Na^+_{total} - Na^+_{soil}) \quad (2)$$

where Cl^-_{soil} and Na^+_{soil} were calculated from Ca^{2+} concentrations using the Cl^-/Ca^{2+} and Na^+/Ca^{2+} mass ratio of the Ca^{2+} in the dry season of 2009, when the $SO_4^{2-}exc/SO_4^{2-}$ ratio was lower than 10%, which indicates low acid deposition.

Table 1. Method detection limit (MDL) and mean concentrations measured by ion chromatography (IC) and inductively coupled plasma sector field mass spectrometry (ICP-SFMS).

	Unit	Method blank	MDL	Mean 1999–2016
Na^+	ng g^{-1}	4.4	1.9	30.9
K^+	ng g^{-1}	1.0	1.1	12.7
Mg^{2+}	ng g^{-1}	5.3	0.9	11.4
Ca^{2+}	ng g^{-1}	16.7	21.1	88.9
Cl^-	ng g^{-1}	10.9	4.9	56.7
NO_3^-	ng g^{-1}	14.9	4.4	185.9
SO_4^{2-}	ng g^{-1}	35.2	57.3	381.8
Li	pg g^{-1}	15.8	4.4	101.5
Na	pg g^{-1}	403	6213	39581
Mg	pg g^{-1}	797	2269	18620
Al	pg g^{-1}	247	2713	39855
Si	pg g^{-1}	42523	39516	219292
S	pg g^{-1}	823	2065	182636
K	pg g^{-1}	872	4422	26022
Ca	pg g^{-1}	2547	3977	58609
Sc	pg g^{-1}	2.2	0.30	2.34
Ti	pg g^{-1}	49.8	557	3580
V	pg g^{-1}	0.8	10.5	68.7
Cr	pg g^{-1}	3.7	7.7	48.8
Mn	pg g^{-1}	32.0	114	2076
Fe	pg g^{-1}	476	8142	52082
Co	pg g^{-1}	0.20	2.2	33.1
Cu	pg g^{-1}	50.8	57.7	620
Zn	pg g^{-1}	235	417	1321
As	pg g^{-1}	3.6	18.4	208.4
Sr	pg g^{-1}	3.4	48.8	634
Ag	pg g^{-1}	0.6	0.5	2.96
Cd	pg g^{-1}	0.5	1.3	8.3
Cs	pg g^{-1}	0.4	1.6	30.6
Ba	pg g^{-1}	32.2	258	1512
La	pg g^{-1}	0.1	1.1	7.34
Ce	pg g^{-1}	0.1	2.1	14.9
Pr	pg g^{-1}	0.01	0.3	1.73
Pb	pg g^{-1}	2.9	5.1	234.8
Bi	pg g^{-1}	0.2	0.5	9.44
U	pg g^{-1}	0.1	0.1	3.9

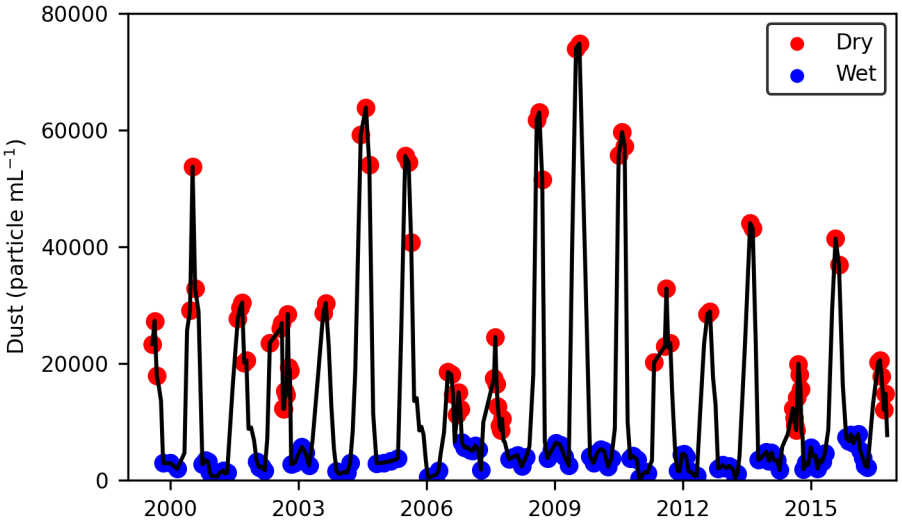

Figure 2. Seasonal classification of Illimani samples into wet (blue dots) and dry (red dots) seasons based on the dust record from (Lindau et al., 2020).

2.3 Seasonally Resolved Chronology and Climate Records

The annual signal in ice cores from Illimani is considered to be largely preserved because precipitation and ablation seasons are relatively distinct (De Angelis et al., 2003). During the dry season, post-depositional processes such as sublimation can significantly perturb the chemical composition of the surface snow (Ginot et al., 2001). However, the sublimation rate at the Illimani site during the dry season of 2001 was -0.7 mm w.e. d^{-1}, whereas a significantly higher snow accumulation (21 cm) occurred during this same period (De Angelis et al., 2003; Wagnon et al., 2003). Thus, a detailed stratigraphy based on the combination of three strong seasonal signals (dust particle concentration, Ca^{2+}, and water stable isotopes) allowed the identification of annual layers along the profile and provided a year-by-year dating of the IL2017 firn core (Lindau et al., 2020). The IL2017 chronology covers the period from 1999 to 2016. Then, data were classified by season following the procedures in Lindau et al. (2020) and Correia et al. (2003) by individually grouping the samples into three categories ("dry," "wet," and "transition") according to dating and dust concentration levels (Figure 2). We obtained 73 (28%) cases of dry samples and 126 (49%) of wet samples.

We used in situ monthly precipitation from four rain-gauge stations located in the Bolivian Altiplano (El Alto, Calacoto, Patacamaya, and Oruro) and one in the Bolivian Amazon (San Borja, Figure 1) over the 1999–2016 period obtained from the Bolivian National Service of Meteorology and Hydrology (SENAMHI) network (www.senamhi.gob.bo/sismet) with monthly resolution. For the precipitation records from the Altiplano, the seasonal variability was eliminated by subtracting the monthly mean of the respective time series in each month. Then, each time series was normalized using its mean and standard deviation values. Finally, we calculated the principal components (PC) of precipitation in the Bolivian Altiplano. The first PC (PC1r) explained 62% of the total precipitation variance. The high correlations ($r > 0.7$, p-value < 0.01) obtained for all stations indicate that the area we chose was influenced by a common mode of rainfall variability.

The reanalysis data set from the European Center for Medium Range Weather Forecasts (ECMWF, ERA5) and ERA-Interim were obtained at the KMNI Climate Explorer (http://climexp.knmi.nl/getindices) and the Climate Reanalyzer (https://climatereanalyzer.org),

respectively, with monthly resolution. Backward and forward air mass trajectories were calculated using HYSPLIT (https://www.ready.noaa.gov/). The NOAA Global Data Assimilation System data at 1° x 1° resolution were used as meteorological input for HYSPLIT.

3 Results and Discussion

3.1 Comparison with Records from the 20^{th} Century

To relate the elemental and ionic records in Illimani during the 1999–2016 period (IL2017) with other ice core records, we calculated a decadal (2005–2015) mean concentration for each element. Table 2 shows an equal resolution comparison between the IL2017 decadal mean and records covering the 1980–1990 period in both Illimani (IL1999) (Correia et al., 2003; De Angelis et al., 2003) and Quelccaya (Uglietti et al., 2015) ice cores. We observed a difference of one order of magnitude between the Al concentrations of the Illimani records. This is possibly related to differences in sample acidification (Section 2.2). An acid digestion method was applied by Correia et al. (2003), and we believe this was one of the major causes for the differences observed for Al, Co, and Cu. Conversely, for elements that are less sensitive to different acidification conditions (e.g., Mn, As, Pb) (Uglietti et al., 2014), we observed minor differences. In fact, the major ions showed slightly higher concentrations during the early 21^{st} century (Table 2).

Despite the variations in elemental concentrations due to distinct leaching, EF interpretation is less affected as larger variations are allowed to classify sources in crustal or non-crustal (EF larger or smaller than 10) (Uglietti et al., 2014). Non-crustal elements for all IL2017, IL1999, and Quelccaya were As, Cu, and Cd (Table 2). Interestingly, Cr EF showed a reduction in the 21^{st} century as it was >10 for both IL1999 and Quelccaya, but in IL2017, it was close to unity (Table 2). The presence of anthropogenic Cr in an ice core from the Alps was attributed to iron, steel, and ferro-alloy production (Van De Velde et al., 1999); ferromolybdenum is produced in northern Chile as a sub-product of Cu production. An unprecedented rise in Cu EF (over the last two millennia) was observed during the second half of the 20^{th} century in Illimani, followed by a decrease since the 1990s due to the regulation of smelter emissions in Chile (Eichler et al., 2017). Thus, according to our record, Cr was efficiently controlled by reduced emission rates from smelters, although other mining and smelter-related elements such as Cu, Cd, Zn, As, and Ag are still enriched in Illimani. Indeed, we observed a considerable anthropogenic contribution for Zn, As, and Ag in Illimani during both the 20^{th} and 21^{st} centuries (Table 2).

Bi was not analyzed in IL1999, and in Quelccaya it showed a low EF during the 20^{th} century (Table 2). Conversely, it was enriched (Bi EF = 22) in an ice core from Sajama (Figure 1) during the late 20^{th} century (Hong et al., 2004). Bi might also be enriched by volcanic fallout; in that case, it would probably be related to a higher S EF (Ferrari et al., 2000; Kaspari et al., 2009). Although S was analyzed only in IL2017, the high mean EF observed in Table 2 was expected because S might be associated with SO_2 sourced by smelting, fossil fuel combustion, and biomass burning, which, in turn, had an impact on records from Illimani (Eichler et al., 2015; Brugger et al., 2019; Osmont et al., 2019).

3.2 Potential Volcanic Signatures

Sulfur EF showed a good correspondence with $SO_4^{2-}exc$, showing peaks when $SO_4^{2-}exc/SO_4^{2-}$ was higher than 75% (Figure 3). In ice cores, $SO_4^{2-}exc$ is often used as a proxy for volcanic eruptions. Furthermore, if $SO_4^{2-}exc$ variability is related to volcanic eruptions, the deposition of halogen gases such as HCl would also be expected (De Angelis et al., 2003). We observed a spike for both Cl^-exc and $SO_4^{2-}exc$ only during the transition and wet seasons of 2014/15. In September 2014, SO_2 emissions from the Nyamuragira-Nyiragongo volcanoes (1°24′S; 29°12′E, 3058 m a.s.l, Democratic Republic of the Congo) crossed the

Table 2. Decadal comparison between 21^{st}-century records from Illimani (ILL2017) and 20^{th}-century records from Illimani (ILL1999) and Quelccaya (QCY). Enrichment factors (EF) higher than 10 are shown in bold.

	2005–2015		1980–1990			
	IL2017		IL1999		QCY	
	Conc (pg g^{-1})	EF	Conc (pg g^{-1})	EF	Conc (pg g^{-1})	EF
Li	102	2.4	216	4.1		
Na	39829	1.0	63145	1.0		
Mg	19179	0.7	29907	0.9		
Al	40409	0.3	194292	1.0	51476	1.2
S	166195	**121**				
K	26094	0.5	88962	1.3		
Ca	55335	1.1	82546	1.3		
Sc	2.27	0.2	39.4	2.3		
Ti	3773	0.5	13389	1.6	2302	0.6
V	70.5	0.6	298	1.6	80.9	2.2
Cr	49	0.7	2136	**26**	82.2	**11**
Mn	2026	2.0	3116	2.6		
Fe	57125	0.9	105073	1.3	43932	1.0
Co	31.9	1.6	375	**15**	17.4	4.0
Cu	611	**27**	4276	**136**	248	**22**
Zn	1297	**14**	3533	**34**		
As	216	**72**	668	**159**	147	2.7
Sr	640	1.0	1105	1.5		
Ag	3.11	**33**	3.52	**34**	1.96	8.0
Cd	8.14	**48**	16.1	**70**	4.55	**70**
Cs	30.7	2.9	43.2	3.0		
Ba	1626	1.0	2432	1.5		
La	8.14	0.1	111	1.4		
Ce	16.2	0.1	235	1.4		
Pr	1.92	0.1	25.0	1.6		
Pb	231	7.1	364	9.3	313	6.3
Bi	10.2	**52**			9.95	2.3
U	3.88	0.8	10.4	1.7	10.4	0.3
	Conc (ng g^{-1})		Conc (ng g^{-1})			
Na^+	30.6		18.4			
K^+	11.8		11.3			
Mg^{2+}	11.1		6.0			
Ca^{2+}	86.5		46.5			
Cl^-	54.8		33.5			
NO_3^-	177		138			
SO_4^{2-}	349		325			

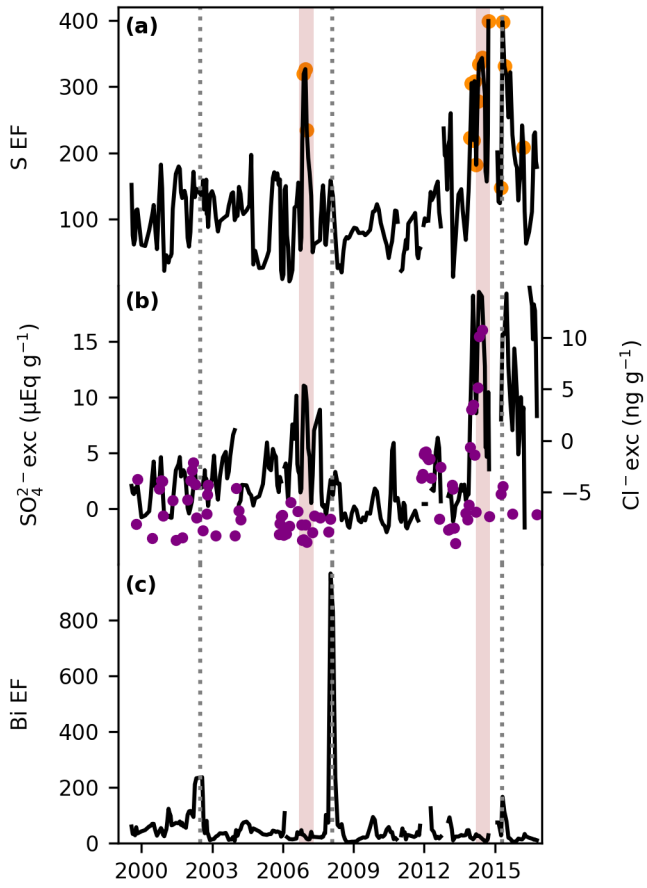

Figure 3. Volcanic proxy records, all data represent three-sample mean values. (a) The enrichment factor (EF) variability for S, the orange dots indicate periods when the excess of SO_4^{2-} represented more than 75% of the total SO_4^{2-} concentration. (b) Both the SO_4^{2-} *exc* (black line) and the excess of Cl^- (purple dots). The vertical brown bands in both 2006 and 2014 indicate the probable volcanic signals of the Rabuk and Nyamuragira-Nyiragongo eruptions, respectively. (c) The EF for Bi, highlighting the period for its major spikes (vertical dotted line).

Atlantic Ocean (Figure S1), and were detected at the Amazon Tall Tower Observatory (ATTO, Figure 1) by an anomalously high atmospheric SO_4^{2-} concentration (Saturno et al., 2018). Back trajectories indicate that the SO_2 plume that arrived in ATTO could have reached Illimani as air parcels over Illimani were mostly from the northeast (Figure 4), thus probably carrying aerosols from the Amazon basin (Chauvigné et al., 2019).

In addition, Figure 3a shows a spike for both S EF and SO_4^{2-} *exc* during the wet season of 2006/07. In October 2006, the Rabaul volcano (4°16′S; 152°12′E, Papua New Guinea) emitted 31 kt of SO_2 (VEI 4), as estimated by the Ozone Monitoring Instrument on the Aura satellite (NASA). The plume was advected eastward, probably reaching South America (Figure S2). Therefore, we consider that the 2006/07 S EF peak was most probably related to the Rabaul eruption. In 2015, another S EF peak was observed, as shown in Figure 3a; this time, we also observed a Bi EF peak. In April 2015, a VEI 4 eruption occurred in the Cabulco volcano (41°19′S; 72°37′W, Chile); however, satel-

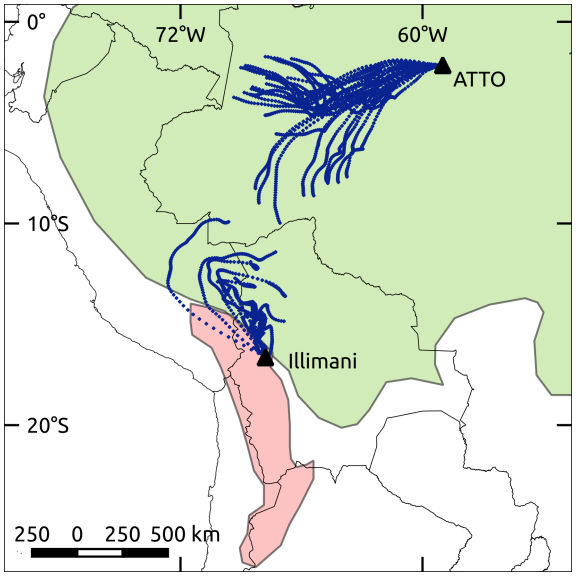

Figure 4. Six-hour air mass trajectories for the September 16–19, 2014 period (blue lines). Backward trajectories over Illimani started at 6350 m above the sea level (a.s.l.). Forward trajectories over ATTO started at 1500 m a.s.l. The green and red areas represent the Amazon basin and the Altiplano, respectively.

lite observations indicate that the SO_2 plume advected toward the Atlantic Ocean due to predominant westerly winds over that latitude, thus not affecting the Illimani region.

Bi EF showed its most prominent peak for the 2007–08 period, which might indicate a volcanic input. However, there is no evidence for a strong tropical or South American volcanic eruption, supporting the occurrence of such a signal during that period. Similar to the observations for the Cabulco SO_2 plume, emissions from the 2008 eruption (VEI 4) of the Chaitén volcano (42°50′S; 72°38′W, Chile) advected toward the Atlantic Ocean. Moreover, we observed a higher Bi enrichment in 2002, contemporary to another Nyiragongo eruption; however, the absence of a S signal suggests that the plume did not reach Illimani.

In fact, Bi is strongly influenced by anthropogenic sources such as fossil fuel combustion and the manufacturing of alloys (Ferrari et al., 2000). In Illimani, Bi EF was significantly correlated with EFs of mining emission-sourced elements such as As, Cd, and Cu (Table S1). It is estimated that approximately 70% of the worldwide atmospheric anthropogenic emissions of Cd and Cu are related to non-ferrous metal production (Pacyna & Pacyna, 2001). The EF for Cu showed a higher variability until 2008, followed by a decrease that agrees with the amount of Cu processed by both smelting and fire refining in Chile (Figure 5). These processes emit large quantities of metals to the atmosphere, and since 2012, they are less used in Chile, according to the Chilean Copper Commission (COCHILCO).

3.3 Altiplano-Related Signal

We observed a common seasonality for the analyzed soluble species during the majority of the 1999–2016 period (Figure 6a; Figure S3). This is expected as the extreme seasonality of precipitation over the Altiplano promotes a well-defined oscillatory pattern in aerosol concentration variability in ice cores from Illimani (Correia et al., 2003; Knüsel et al., 2005; Osmont et al., 2019; Lindau et al., 2020). At this site, approximately 70% of annual precipitation occurs during the wet season (austral summer) and corresponds to the less concentrated snow layers (De Angelis et al., 2003). Furthermore, these

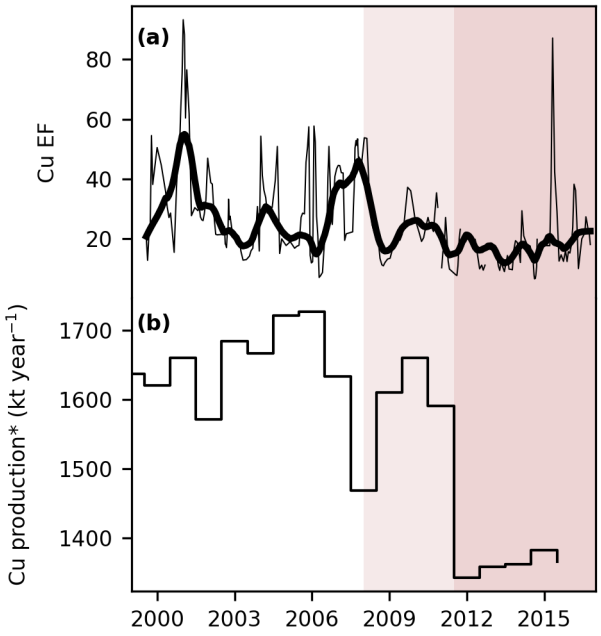

Figure 5. Comparison between the copper enrichment record and production. (a) The thinner line represents the three-sample mean Cu enrichment factor (EF) variability, and the thicker line denotes data smoothed by the LOWESS algorithm (1-year window, approximately). (b) Cu production in Chile, considering only the processes of smelting and fire refining, was obtained from COCHILCO (http://www.cochilco.cl). The lighter brown band represents a first decrease for both Cu EF and production, and the darker brown band denotes the greater decrease in Cu production by both smelting and fire refining.

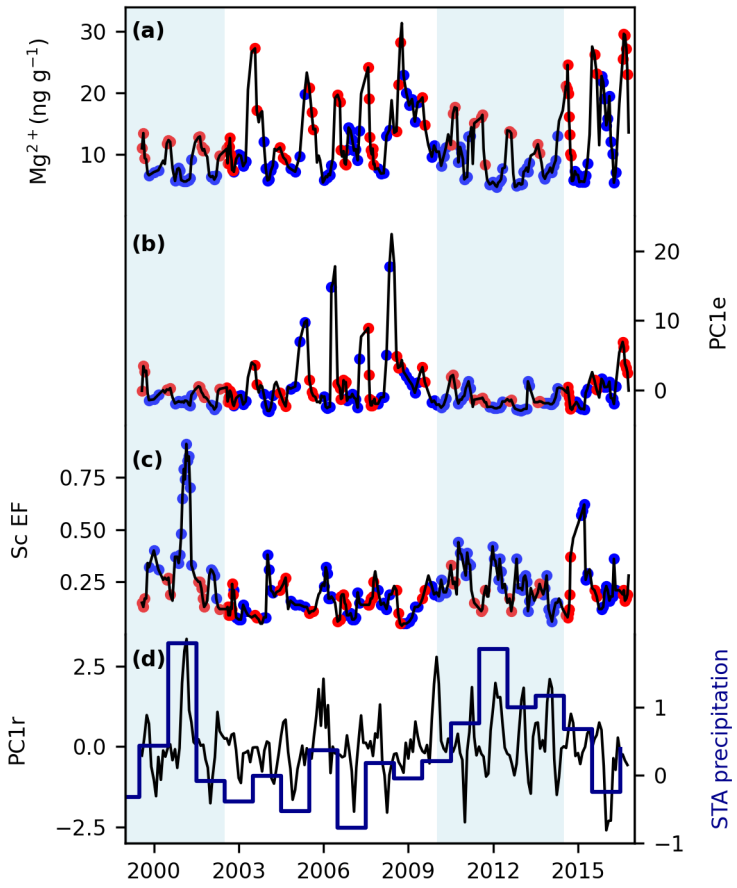

Figure 6. Responses of soluble magnesium (a), the first principal component of elemental concentrations (b), and scandium enrichment factor (c) to the first principal component of monthly precipitation variability over the Altiplano near Illimani (black line), and to annual precipitation (blue line) over the southern tropical Andes (d). Red and blue dots denote samples classified as "dry" and "wet," respectively. Data in (a), (b), and (c) were smoothed by three-sample means. Vertical blue bands represent wetter periods discussed in the text.

authors observed that large concentration peaks occurred during the dry season (austral winter) for most of the studied soluble species due to dry deposition processes and precipitation of heavily loaded snow. Such a seasonal pattern, represented by Mg^{2+} in Figure 6a, is consistent with satellite observations showing higher dust emissions from the Altiplano occurring during the austral winter (Prospero et al., 2002; Gaiero et al., 2013).

Elemental concentrations exhibited a seasonal behavior similar to that observed for major ions. The first PC for elemental concentrations (PC1e, Figure 6b) explains 74% of the total variance, being strongly related ($r > 0.7$) to most of the elements, as well as correlated at the 95% level with all the major ions. However, PC1e showed spikes during the wet season, which might be related to periods of enhanced deposition of anthropogenically sourced aerosols. Indeed, Table S2 shows that PC1e is associated ($r > 0.9$) with highly enriched elements such as As (mean EF of 69) and Cu (29). To avoid data

interpolation, only the detected elements above the MDL in more than 75% of the samples (a total of 17 elements, Table S2) were considered for PC analyses.

The coherence between elemental concentrations was also observed for the EFs. For example, 70% of the EFs were correlated at the 95% level to Sc EF. This crustal-sourced element shows an increased EF during the wet season (Figure 6c). The Sc enrichment in atmospheric aerosols was related to differences in mineral proportions, probably containing little quartz and feldspars that are depleted in Sc, and more abundant clay minerals (Ferrat et al., 2011). This agrees with mineralogical data from Illimani dust, which showed a higher occurrence of aerodynamic plate-like phyllosilicates during the wet season owing to stronger scavenging caused by heavier precipitation (Lindau et al., 2020). Correia et al. (2003) proposed that during the dry season, the aerosol reaching Illimani tends to be closer to soil dust, while during the wet season, regional soil dust aerosols are more efficiently removed than fine, remotely transported aerosols from other sources. This is also observed on an interannual timescale.

As expected, precipitation over the Altiplano near Illimani (PC1r) during the 1999–2016 period shows a similar variability to the southern tropical Andes precipitation (Figure 6d) (Segura et al., 2019, 2020). The wettest year was 2001, followed by a drier period from 2003 to 2010, and then a wetter period from 2010 to 2014 (Figure 6d). Accordingly, the Sc EF is greater during these wetter periods. Conversely, higher elemental and ionic concentrations occurred within the 2003–2010 period. The 1999–2001 summer period featured a more intense and southward-positioned Bolivian High (Figure S4), favoring the transport of moist air from the Amazon lowlands toward the tropical Andes (Garreaud, 1999; Segura et al., 2019). During the summer of 2012, the upward motion over the western Amazon basin was caused by enhanced convection over this region due to the strength of low-level northerlies originating over the tropical Northern Atlantic (Segura et al., 2020).

3.4 Relationship with Atmospheric Circulation over the Amazon Basin

We observed that S enrichment was related to increased atmospheric SO_2 over Illimani, with only volcanic contribution in 2006 and 2014, although the S EF record also showed spikes in 2015 (Section 3.2). Thus, we expect that S EF is related to biomass burning in the lowlands eastward Illimani. Fires over Bolivia, Brazil, and Paraguay during August and September cause changes in aerosol optical properties in Chacaltaya (Chauvigné et al., 2019), as well as increased refractive black carbon (rBC) concentrations in Illimani (Osmont et al., 2019). However, the number of fire spots in that area was lower in 2015 than in 2004, 2007, and 2010 (Figure S5) when no dry season S EF peaks were observed. Interestingly, the dry season S EF showed a good correlation with the dry season Mn EF (Figure 7, $r = 0.64$, $p < 0.001$).

The Mn EF, in turn, showed significant correlations at the 95% level with the low-level circulation over the Amazon basin during the austral winter (Figure 8), which is related to the SALLJ. In Figure 8, the more intense the SALLJ, the greater the enrichment in Mn. This is represented by its relationship with northerly wind anomalies at 850 hPa along the eastern slope of the southern tropical Andes (Figure 8), and to easterly wind anomalies at 850 hPa over the northeastern Amazon basin and westerly anomalies along the eastern slope of the southern tropical Andes (Figure S6). Enhanced SALLJ increases orographic precipitation over the Bolivian Eastern Cordillera (Jones, 2019). In accordance, Mn EF showed a positive correlation ($r = 0.53$, $p < 0.05$) with precipitation over the eastern slope of the Bolivian Eastern Cordillera during the austral winter, as indicated by meteorological observations in San Borja (Figure 1). This orographic precipitation potentially carries aerosols from the Amazon basin up to Illimani. Moreover, Thompson et al. (2013) observed that moisture bringing Amazon-sourced biogenic ammonium aerosol to Illimani arrives via winds at the 500-hPa level originating from east-southeast. We observed a positive correlation between the Mn EF and the relative humidity eastward at the 500-hPa level (Figure S7).

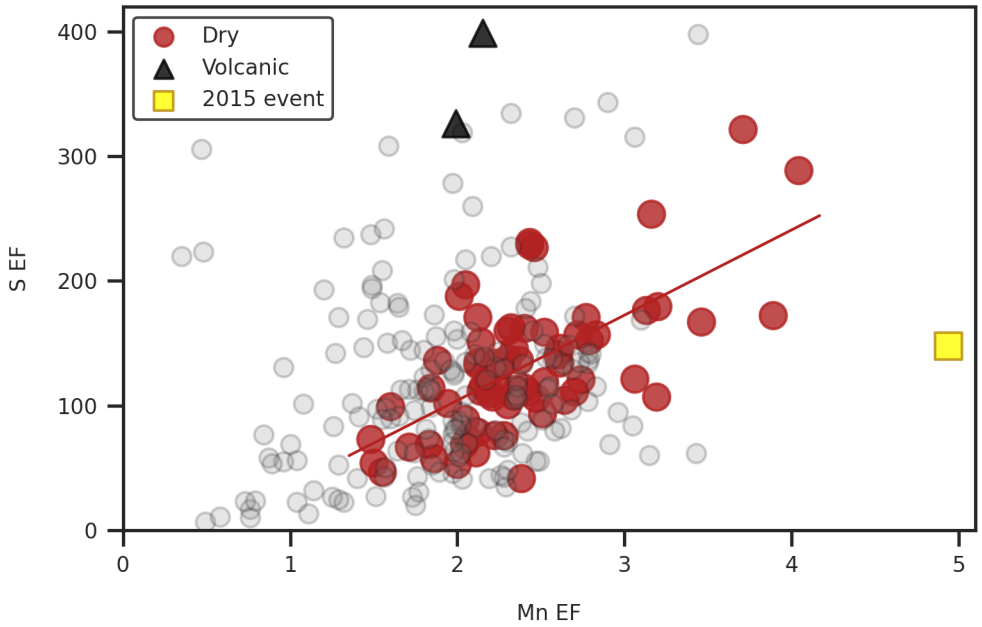

Figure 7. Linear relationship (indicated by the red line) between Mn and S enrichment factors (EFs) during the dry season (red circles). EFs related to volcanic events and to the 2015 dust event discussed in the text are represented by the black triangles and yellow square, respectively. Light gray dots in the background are the wet and transition season EFs.

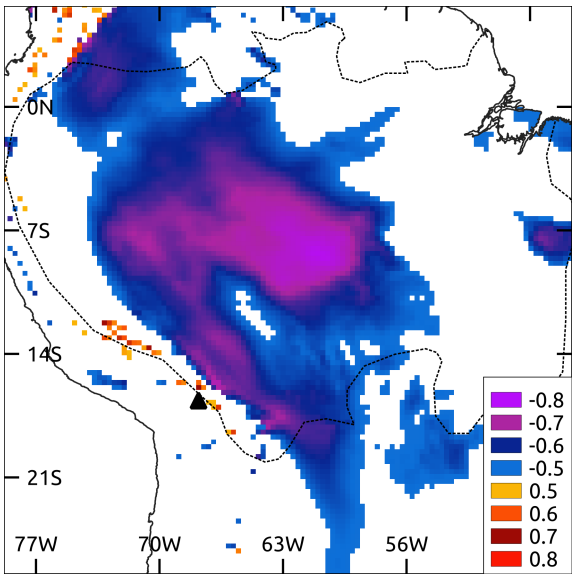

Figure 8. Spatial correlations (significant at the 95% level) during the months MJJAS (2000–2016 period) between the monthly resampled Mn enrichment factor and meridional winds at the 850-hPa level (ERA5 reanalysis). The black triangle indicates the Illimani site, and the dotted line delimits the Amazon basin.

Therefore, we believe that the dry season S EF signal is mainly controlled by atmospheric circulation over the Amazon basin. In fact, during the dry season of 2015, SALLJ intensified in comparison to the 1999–2016 period (Figure S8). This role of atmospheric circulation controlling the deposition of biomass burning proxies at Illimani has implications for interpreting rBC records in ice cores from the Andean Eastern Cordillera. Moreover, the use of Mn EF as a proxy for the austral winter intensity of the SALLJ might have implications for studying severe weather due to convective systems during the dry season in southeastern Brazil, already related to intense low-level jet flow (Rehbein et al., 2018).

We call attention to the 2014/15 wet season Mn EF peak that was unprecedented over the 1999–2016 record (Figure 7), and were followed by greater spikes of Co and Fe EF (Figure S9). On April 5 and 6 of 2015, a dust plume from the Saharan–Sahel region was detected in central Amazonia, which was supported by satellite data and air mass back trajectories, leading to peak concentrations of Fe (Rizzolo et al., 2017). According to our chronology, spikes for Co, Fe, and Mn occurred during that same period. Furthermore, air mass back trajectories for Illimani during that period indicated a predominant north-northeast direction (Figure S10), and therefore, most probably carry aerosols from the northern Amazon basin. The African dust aerosol reaching Central Amazonia is carried by northeasterly trade winds (Swap et al., 1992; Yu et al., 2015), and is enriched in crustal and biomass burning-related elements, reflecting higher concentrations of Fe, Mn, and S (Formenti et al., 2011; Moran-Zuloaga et al., 2018). The Co EF spike, by its turn, might be associated with continental biogenic sources, biomass burning, and combustion processes (Nriagu, 1989; Van De Velde et al., 1999). Interestingly, Co EF was close to unity along the IL2017 record, indicating that it was mostly crustal sourced. Therefore, we consider that the presence of African dust in tropical Andean glaciers deserves future geochemical investigation.

4 Conclusions

The early 21^{st}-century EF record of Illimani indicates lower anthropogenic contamination for Cr than during the late 20^{th} century, probably due to lower emissions from mining-related activities. Indeed, a decrease in Chilean copper production via smelting and fire refining since 2008 seems to be reflected in reduced Cd and Cu EFs. Sulfur, by its turn, was highly enriched in Illimani along the 1999–2016 record (mean of 124) due to high SO_2 emissions from various anthropogenic sources. Moreover, we suggest that two S EF spikes (2006/07 and 2014) were due to volcanic eruptions.

Aerosols over the Central Amazon region can be transported to southern tropical Andes by SALLJs, which promote their uplift at the eastern Bolivian Andes. This was best reflected by Mn EF variability during the dry season (May to September), which was correlated at the 95% level to both zonal and meridional winds at the 850-hPa level and to 500 hPa relative humidity over the lowlands eastward Illimani. Furthermore, we attributed the enrichment for both Mn and S during 2015 to the enhanced SALLJ in comparison to the rest of the IL2017 record. Back trajectories and unprecedented EFs for Co, Fe, and Mn in IL2017 suggest that a dust plume from Africa might be recorded in the snow layers. We consider that this topic deserves further investigation.

Overall, concentrations for most anthropogenic and crustal-sourced elements and major ions featured a well-defined seasonal variability, modulated by the clear separation of wet and dry seasons over the southern tropical Andes. Sc was enriched during wetter periods, probably because the stronger scavenging favored by the deposition of minerals more concentrated in that element.

Acknowledgments

We thank the drillers S. Kutuzov, L. Piard, B. Jourdain, the entire operation team, and the support of the IRD office in Bolivia. Operations at Illimani were part of the Ice Memory project financed by IRD at the Université Grenoble Alpes, CNRS, IPEV, and UMSA,

and by a sponsorship from the Université Grenoble Alpes Foundation. We thank B. Delmonte, G. Baccolo, and V. Maggi for their support at EuroCold, Italy. This investigation is a contribution of the Brazilian National Institute for Cryospheric Sciences (Process CNPq 465680/2014-3). It was partially funded by NSF project 1600018 and by the Brazilian CAPES, project 88887.136384/2017-00. F.G.L. Lindau thanks CNPq for his scholarship (Processes 141013/2015-0 and 200496/2017-4). The data presented in this work will be archived at the National Oceanic and Atmospheric Administration World Data Center-A for Paleoclimatology.

References

Brugger, S. O., Gobet, E., Osmont, D., Behling, H., Fontana, S. L., Hooghiemstra, H., ... Tinner, W. (2019). Tropical Andean glacier reveals colonial legacy in modern mountain ecosystems. *Quaternary Science Reviews*, *220*, 1–13. doi: 10.1016/j.quascirev.2019.06.032

Chauvigné, A., Diego, A., Marcos, A., Patrick, G., Radovan, K., Griša, M., ... Laj, P. (2019). Biomass-burning and urban emission impacts in the Andes Cordillera region based on in-situ measurements from the Chacaltaya observatory, Bolivia (5240 m a.s.l.). *Atmospheric Chemistry and Physics*, *19*, 14805–14824. doi: 10.5194/acp-2019-510

Correia, A., Freydier, R., Delmas, R. J., Simões, J. C., Taupin, J. D., Dupré, B., & Artaxo, P. (2003). Trace elements in South America aerosol during 20th century inferred from a Nevado Illimani ice core, Eastern Bolivian Andes (6350 m asl). *Atmospheric Chemistry and Physics*, *3*(5), 1337–1352. doi: 10.5194/acp-3-1337-2003

De Angelis, M., Simões, J., Bonnaveira, H., Taupin, J. D., & Delmas, R. J. (2003). Volcanic eruptions recorded in the Illimani ice core (Bolivia): 1918-1998 and Tambora periods. *Atmospheric Chemistry and Physics*, *3*(5), 1725–1741. doi: 10.5194/acp-3-1725-2003

de Magalhães, N., Evangelista, H., Condom, T., Rabatel, A., & Ginot, P. (2019). Amazonian Biomass Burning Enhances Tropical Andean Glaciers Melting. *Scientific Reports*, *9*(1), 1–12. doi: 10.1038/s41598-019-53284-1

Eichler, A., Gramlich, G., Kellerhals, T., Tobler, L., Rehren, T., & Schwikowski, M. (2017). Ice-core evidence of earliest extensive copper metallurgy in the Andes 2700 years ago. *Scientific Reports*, *7*, 41855. doi: 10.1038/srep41855

Eichler, A., Gramlich, G., Kellerhals, T., Tobler, L., & Schwikowski, M. (2015). Pb pollution from leaded gasoline in South America in the context of a 2000-year metallurgical history. *Science Advances*, *1*, e1400196. doi: 10.1126/sciadv.1400196

Espinoza, J. C., Garreaud, R., Poveda, G., Arias, P. A., Molina-Carpio, J., Masiokas, M., ... Scaff, L. (2020). Hydroclimate of the Andes Part I: Main Climatic Features. *Frontiers in Earth Science*, *8*, 1–20. doi: 10.3389/feart.2020.00064

Ferrari, C. P., Hong, S., Van De Velde, K., Boutron, C. F., Rudniev, S. N., Bolshov, M., ... Rosman, K. J. (2000). Natural and anthropogenic bismuth in Central Greenland. *Atmospheric Environment*, *34*(6), 941–948. doi: 10.1016/S1352-2310(99)00257-5

Ferrat, M., Weiss, D. J., Strekopytov, S., Dong, S., Chen, H., Najorka, J., ... Sinha, R. (2011). Improved provenance tracing of Asian dust sources using rare earth elements and selected trace elements for palaeomonsoon studies on the eastern Tibetan Plateau. *Geochimica et Cosmochimica Acta*, *75*(21), 6374–6399. doi: 10.1016/j.gca.2011.08.025

Formenti, P., Schütz, L., Balkanski, Y., Desboeufs, K., Ebert, M., Kandler, K., ... Zhang, D. (2011). Recent progress in understanding physical and chemical properties of African and Asian mineral dust. *Atmospheric Chemistry and*

Physics, *11*(16), 8231–8256. doi: 10.5194/acp-11-8231-2011

Gabrielli, P., Wegner, A., Roxana Sierra-Hernández, M., Beaudon, E., Davis, M., Barker, J. D., & Thompson, L. G. (2020). Early atmospheric contamination on the top of the Himalayas since the onset of the European Industrial Revolution. *PNAS*, *117*(8), 3967–3973. doi: 10.1073/pnas.1910485117

Gaiero, D. M., Simonella, L., Gassó, S., Gili, S., Stein, A. F., Sosa, P., ... Marelli, H. (2013). Ground/satellite observations and atmospheric modeling of dust storms originating in the high Puna-Altiplano deserts (South America): Implications for the interpretation of paleoclimatic archives. *Journal of Geophysical Research Atmospheres*, *118*(9), 3817–3831. doi: 10.1002/jgrd.500362013

Garreaud, R. D. (1999). Multiscale Analysis of the Summertime Precipitation over the Central Andes. *Monthly Weather Review*, *127*(5), 901–921. doi: 10.1175/1520-0493(1999)127⟨0901:MAOTSP⟩2.0.CO;2

Ginot, P., Kull, C., Schwikowski, M., Schotterer, U., & Gäggeler, H. W. (2001). Effects of postdepositional processes on snow composition of a subtropical glacier (Cerro Tapado, Chilean Andes). *Journal of Geophysical Research*, *106*(D23), 32375. doi: 10.1029/2000JD000071

Hong, S., Barbante, C., Boutron, C., Gabrielli, P., Gaspari, V., Cescon, P., ... Maurice-Bourgoin, L. (2004). Atmospheric heavy metals in tropical South America during the past 22 000 years recorded in a high altitude ice core from Sajama, Bolivia. *Journal of Environmental Monitoring*, *6*(4), 322–326. doi: 10.1039/b314251e

Jones, C. (2019). Recent changes in the South America low-level jet. *Climate and Atmospheric Science*, *2*(1), 1–8. doi: 10.1038/s41612-019-0077-5

Kaspari, S., Mayewski, P. A., Handley, M., Osterberg, E., Kang, S., Sneed, S., ... Qin, D. (2009). Recent increases in atmospheric concentrations of Bi, U, Cs, S and Ca from a 350-year Mount Everest ice core record. *Journal of Geophysical Research Atmospheres*, *114*(4). doi: 10.1029/2008JD011088

Kellerhals, T., Brütsch, S., Sigl, M., Knüsel, S., Gäggeler, H. W., & Schwikowski, M. (2010). Ammonium concentration in ice cores: A new proxy for regional temperature reconstruction? *Journal of Geophysical Research Atmospheres*, *115*(16), 1–8. doi: 10.1029/2009JD012603

Knüsel, S., Brütsch, S., Henderson, K. A., Palmer, A. S., & Schwikowski, M. (2005). ENSO signals of the twentieth century in an ice core from Nevado Illimani, Bolivia. *Journal of Geophysical Research D: Atmospheres*, *110*(1), 1–14. doi: 10.1029/2004JD005420

Knüsel, S., Ginot, P., Schotterer, U., Schwikowski, M., Gäggeler, H. W., Francou, B., ... Taupin, J. D. (2003). Dating of two nearby ice cores from the Illimani, Bolivia. *Journal of Geophysical Research*, *108*(D6), 4181. doi: 10.1029/2001JD002028

Lenters, J. D., & Cook, K. H. (1997). On the Origin of the Bolivian High and Related Circulation Features of the South American Climate. *Journal of the Atmospheric Sciences*, *54*(5), 656–678. doi: 10.1175/1520-0469(1997)054⟨0656:OTOOTB⟩2.0.CO;2

Lindau, F. G. L., Simões, J. C., Delmonte, B., Ginot, P., Baccolo, G., Paleari, C. I., ... Andò, S. (2020). Giant dust particles at Nevado Illimani: a proxy of summertime deep convection over the Bolivian Altiplano. *The Cryosphere Discussions*(April), 1–21. doi: 10.5194/tc-2020-55

Marengo, J. A. (2004). Interdecadal variability and trends of rainfall across the Amazon basin. *Theoretical and Applied Climatology*, *78*(1-3), 79–96. doi: 10.1007/s00704-004-0045-8

Moran-Zuloaga, D., Ditas, F., Walter, D., Saturno, J., Brito, J., Carbone, S., ... Pöhlker, C. (2018). Long-term study on coarse mode aerosols in the Amazon rain forest with the frequent intrusion of Saharan dust plumes. *Atmospheric Chemistry and Physics*, *18*(13), 10055–10088. doi: 10.5194/

484 acp-18-10055-2018
485 Nriagu, J. (1989). A global assessment of natural sources of atmospheric trace met-
486 als. *Nature*, *338*(6210), 47–49. doi: 10.1038/338047a0
487 Osmont, D., Sigl, M., Eichler, A., Jenk, T. M., & Schwikowski, M. (2019). A
488 Holocene black carbon ice-core record of biomass burning in the Amazon
489 Basin from Illimani, Bolivia. *Climate of the Past*, *15*(2), 579–592. doi:
490 10.5194/cp-15-579-2019
491 Osterberg, E. C., Handley, M. J., Sneed, S. B., Mayewski, P. A., & Kreutz, K. J.
492 (2006). Continuous ice core melter system with discrete sampling for major
493 ion, trace element, and stable isotope analyses. *Environmental Science and*
494 *Technology*, *40*(10), 3355–3361. doi: 10.1021/es052536w
495 Pacyna, J. M., & Pacyna, E. G. (2001). An assessment of global and regional emis-
496 sions of trace metals to the atmosphere from anthropogenic sources worldwide.
497 *Environmental Reviews*, *9*(4), 269–298. doi: 10.1139/er-9-4-269
498 Prospero, J. M., Ginoux, P., Torres, O., Nicholson, S. E., & Gill, T. E. (2002).
499 Environmental characterization of global sources of atmospheric soil dust
500 identified with the NIMBUS 7 Total Ozone Mapping Spectrometer (TOMS)
501 absorbing aerosol product. *Reviews of Geophysics*, *40*(1), 1–31. doi:
502 10.1029/2000RG000095
503 Rehbein, A., Dutra, L. M. M., Ambrizzi, T., Da Rocha, R. P., Reboita, M. S., Da
504 Silva, G. A. M., ... Carpenedo, C. B. (2018). Severe Weather Events over
505 Southeastern Brazil during the 2016 Dry Season. *Advances in Meteorology*,
506 *2018*. doi: 10.1155/2018/4878503
507 Rizzolo, J. A., Barbosa, C. G., Borillo, G. C., Godoi, A. F., Souza, R. A., Andreoli,
508 R. V., ... Godoi, R. H. (2017). Soluble iron nutrients in Saharan dust over
509 the central Amazon rainforest. *Atmospheric Chemistry and Physics*, *17*(4),
510 2673–2687. doi: 10.5194/acp-17-2673-2017
511 Saturno, J., Ditas, F., De Vries, M. P., Holanda, B. A., Pöhlker, M. L., Carbone, S.,
512 ... Pöhlker, C. (2018). African volcanic emissions influencing atmospheric
513 aerosols over the Amazon rain forest. *Atmospheric Chemistry and Physics*,
514 *18*(14), 10391–10405. doi: 10.5194/acp-18-10391-2018
515 Schwikowski, M., Döscher, A., Gäggeler, H. W., & Schotterer, U. (1999). Anthro-
516 pogenic versus natural sources of atmospheric sulphate from an Alpine ice
517 core. *Tellus B: Chemical and Physical Meteorology*, *51*(5), 938–951. doi:
518 10.3402/tellusb.v51i5.16506
519 Segura, H., Espinoza, J. C., Junquas, C., Lebel, T., Vuille, M., & Garreaud, R.
520 (2020). Recent changes in the precipitation-driving processes over the southern
521 tropical Andes/western Amazon. *Climate Dynamics*, *54*(5-6), 2613–2631. doi:
522 10.1007/s00382-020-05132-6
523 Segura, H., Junquas, C., Espinoza, J. C., Vuille, M., Jauregui, Y. R., Rabatel, A.,
524 ... Lebel, T. (2019). New insights into the rainfall variability in the tropical
525 Andes on seasonal and interannual time scales. *Climate Dynamics*, *53*(1-2),
526 405–426. doi: 10.1007/s00382-018-4590-8
527 Sen, I. S., & Peucker-Ehrenbrink, B. (2012). Anthropogenic disturbance of element
528 cycles at the Earth's surface. *Environmental Science and Technology*, *46*(16),
529 8601–8609. doi: 10.1021/es301261x
530 Swap, R., Garstang, M., Greco, S., Talbot, R., & Kallberg, P. (1992). Saharan dust
531 in the Amazon Basin. *Tellus, Series B*, *44 B*(2), 133–149. doi: 10.3402/tellusb
532 .v44i2.15434
533 Thompson, L. G., Mosley-Thompson, E., Davis, M. E., Zagorodnov, V. S., Howat,
534 I. M., Mikhalenko, V. N., & Lin, P.-N. (2013). Annually resolved ice core
535 records of tropical climate variability over the past ˜1800 years. *Science*, *340*,
536 945–950. doi: 10.1126/science.1234210
537 Uglietti, C., Gabrielli, P., Cooke, C. A., Vallelonga, P., & Thompson, L. G.
538 (2015). Widespread pollution of the south american atmosphere pre-

dates the industrial revolution by 240 y. *PNAS*, *112*(8), 2349–2354. doi: 10.1073/pnas.1421119112

Uglietti, C., Gabrielli, P., Olesik, J. W., Lutton, A., & Thompson, L. G. (2014). Large variability of trace element mass fractions determined by ICP-SFMS in ice core samples from worldwide high altitude glaciers. *Applied Geochemistry*, *47*, 109–121. doi: 10.1016/j.apgeochem.2014.05.019

Van De Velde, K., Ferrari, C., Barbante, C., Moret, I., Bellomi, T., Hong, S., & Boutron, C. (1999). A 200 year record of atmospheric cobalt, chromium, molybdenum, and antimony in high altitude alpine firn and ice. *Environmental Science and Technology*, *33*(20), 3495–3501. doi: 10.1021/es990066y

Vera, C., Higgins, W., Amador, J., Ambrizzi, T., Garreaud, R., Gochis, D., ... Zhang, C. (2006). Toward a unified view of the American monsoon systems. *Journal of Climate*, *19*(20), 4977–5000. doi: 10.1175/JCLI3896.1

Vimeux, F., Ginot, P., Schwikowski, M., Vuille, M., Hoffmann, G., Thompson, L. G., & Schotterer, U. (2009). Climate variability during the last 1000 years inferred from Andean ice cores: A review of methodology and recent results. *Palaeogeography, Palaeoclimatology, Palaeoecology*, *281*(3-4), 229–241. doi: 10.1016/j.palaeo.2008.03.054

Wagnon, P., Sicart, J. E., Berthier, E., & Chazarin, J. P. (2003). Wintertime high-altitude surface energy balance of a Bolivian glacier, Illimani, 6340 m above sea level. *Journal of Geophysical Research*, *108*(D6), 4177. doi: 10.1029/2002JD002088

Wedepohl, K. H. (1995). The composition of the continental crust. *Geochimica et Cosmochimica Acta*, *59*(7), 1217–1232. doi: 10.1016/0016-7037(95)00038-2

Yu, H., Chin, M., Yuan, T., Bian, H., Remer, L. A., Prospero, J. M., ... Zhao, C. (2015). The fertilizing role of African dust in the Amazon rainforest: A first multiyear assessment based on data from Cloud-Aerosol Lidar and Infrared Pathfinder Satellite Observations. *Geophysical Research Letters*, *42*(6), 1984–1991. doi: 10.1002/2015GL063040